Multi-rate Kalman Filter Design for Electric Vehicles Control based on Onboard Vision System with Uneven Time Delay

Yafei Wang* Binh Minh Nguyen Hiroshi Fujimoto** Yoichi Hori****

** Department of Electrical Engineering, The University of Tokyo, Tokyo, 113-0033 Japan (Tel: 04-7136-3873; e-mail: wang@hori.k.u-tokyo.ac.jp).*
*** Department of Advanced Energy, The University of Tokyo, Chiba, 227-8561 Japan (Tel: 04-7136-3873; e-mail: minh@hori.k.u-tokyo.ac.jp, fujimoto@k.u-tokyo.ac.jp, hori@k.u-tokyo.ac.jp)*

Abstract: Vehicle safety systems have become increasingly popular in modern vehicles, and real time information of vehicle states such as yaw rate, lateral acceleration and lateral position is indispensable for such systems. Yaw rate and acceleration signals can be obtained from onboard gyro/inertial sensors, and vehicle lateral position can be measured by an onboard vision system. Normally, the sampling rate of a camera is much slower compared with that of the other onboard sensors. Moreover, image processing takes time and the time varies depending on captured images and hardware loads (delay time is measurable through time stamp). In case of integrated vehicle motion and position control, however, a unified feedback frequency is desired. Considering the slow control periods of traditional actuators such as hydraulic brakes, many previous studies down-sample the fast rate sensors to adapt the vision device. On the other hand, for electric vehicles, the control period of actuators (motors) is much shorter than the sampling time of a normal camera. To improve the control performance, this research employs a combined vehicle and vision model for lateral position estimation and proposes a multi-rate Kalman filter with reconstructed measurements based on an inter-sample residual estimation technique.

Keywords: Multi-rate Kalman filter, vehicle lateral position, electric vehicle, random measurement delay, motion control, vision system.

1. INTRODUCTION

For vehicle stability control systems, vehicle states such as yaw rate, lateral acceleration and lateral position are considered as key enablers. A yaw moment control algorithm was developed using differential torque of in-wheel-motors (IWMs) for effective vehicle yaw motion stabilization [Fujimoto *et al*. 2006]. Another research tried to control vehicle lateral motion through differential braking [Kim *et al*. 2012]. Meanwhile, automatic steering devices for lane keeping have been extensively investigated by automotive companies and research institutions. For example, some previous studies were surveyed and new methods for lane detection and performance evaluation criteria were proposed [McCall *et al*. 2006]. In another research, stereo vision system was employed to detect lane markers and obstacles on the road [Bertozzi *et al*. 1998]. In case of integrated control of vehicle motion and position, a unified feedback frequency is necessary. However, the sampling rate of a normal camera is much slower compared with that of the other onboard sensors. In addition, image processing time is not constant in practice (because of different incoming images and processing loads). Previous literatures simplify these problems by neglecting delay and down-sampling the overall sampling rate for traditional vehicles using engines and hydraulic systems. For electric vehicles (EVs), the sampling times of traction motors are in millisecond-level. For the enhancement of control performance, faster feedback is desirable. That is, multi-rate issue exists in both state estimation and control for electric vehicles.

A vision-based estimation method for body slip angle was proposed by the authors' group, and a constant visual measurement delay was assumed for the vision system [Wang et al. 2012]. In that research, the delay issue is solved using the state augmentation method [Choi *et al*. 2009]. However, in case of uneven time delay, expansion of system state space equation is not practical due to the varying of delayed steps. In this paper, the measurable uneven delay issue is solved with a residual reconstruction approach, which does not involve state augmentation procedures. Moreover, the aforementioned sampling mismatch of vision system and other onboard sensors is also addressed in the Kalman filter design using an inter-sample residual estimation technique. The proposed multi-rate estimation approach is verified by both simulation and experiment.

2. SYSTEM MODEL AND EXPERIMENTAL SETUPS

1.1 Vehicle Model

For state estimation and control of electric vehicles (EVs), bicycle model considering the differential torque generated by the left and right in-wheel motors (IWMs) is usually employed [Aoki *et al*. 2005].

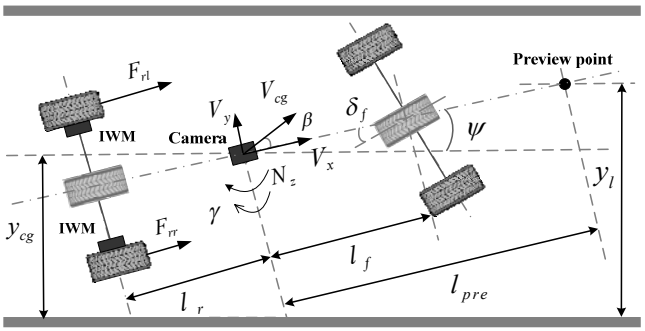

Fig. 1. Combined vehicle and vision models.

The vehicle model used in this research is shown in Fig. 1. The governing equations are given in (1) and (2), where β and γ are the body slip angle and the yaw rate at the vehicle's center of gravity (CoG), respectively, δ_f is the front-steering angle, V_x is the vehicle's longitudinal velocity, V_{cg} is the vehicle's velocity at CoG, m is the vehicle mass, I is the moment of inertia about the yaw axis, C_f and C_r are the cornering stiffness of the front and rear wheels, respectively, l_f and l_r are the distances from the CoG to the front and rear wheels, respectively, and N_z is the yaw moment generated by the differential torque of the rear wheels, which is used as control input in this research.

$$m \cdot V_x \cdot (\dot{\beta} + \gamma) = 2 \cdot C_f \cdot (\delta_f - \frac{l_f}{V_x}\gamma - \beta) + 2 \cdot C_r \cdot (\frac{l_r}{V_x}\gamma - \beta) \quad (1)$$

$$I \cdot \dot{\gamma} = 2 \cdot l_f \cdot C_f \cdot (\delta_f - \frac{l_f}{V_x}\gamma - \beta) - 2 \cdot l_r \cdot C_r \cdot (\frac{l_r}{V_x}\gamma - \beta) + N_z \quad (2)$$

1.2 Vision Model

The vehicle model is independent of road reference, whereas the vision model is obtained from the geometric relationship between the vehicle and the road [Cerone *et al*. 2009]. The vision model is also shown in Fig. 1, where y_l is the lateral offset at a preview point, ψ denotes the heading angle, y_{cg} is the lateral offset at the vehicle's CoG, and l_{pre} is the fixed preview distance that needs to be calibrated beforehand. The gray borders in Fig. 1 are lane makers, and the vision system is located at the vehicle's CoG. In this model, assumptions that the vehicle travels along a straight road and that the onboard vision system detects the lane and provides relative position information were made.

To derive the vision model, ψ and β are assumed to be small. Based on Fig. 1, y_l is approximated as

$$\begin{aligned} y_l &= y_{cg} + l_{pre} \cdot \sin\psi \\ &\approx y_{cg} + l_{pre} \cdot \psi \end{aligned} \quad (3)$$

Then, y_{cg} is derived as (4) based on geometry.

$$\begin{aligned} \dot{y}_{cg} &= V_{cg} \cdot \sin(\beta + \psi) \\ &= V_x / \cos(\beta) \cdot \sin(\beta + \psi) \\ &\approx V_x \cdot (\beta + \psi) \end{aligned} \quad (4)$$

The final equation that describes the body slip angle, yaw rate, and heading angle is obtained by taking the derivative of (3) and substituting (4) into it.

$$\dot{y}_l = V_x \cdot \beta + l_{pre} \cdot \gamma + V_x \cdot \psi \quad (5)$$

Heading angle ψ can be simply modelled as the integration of the yaw rate as

$$\dot{\psi} = \gamma \quad (6)$$

1.3 Combined System Model

Combining (1) to (6) yields a new system that is represented in a continuous state space form as (7). The first two states are modelled by the vehicle model, and the latter two are modelled by the vision model. Clearly, the vision model contains much fewer uncertainties compared with the bicycle model. In the combined vehicle and vision models, the measurable outputs are yaw rate, vehicle heading angle, and lateral offset at the preview point. The body slip angle is still observable using only visual information, which provides estimation redundancy.

$$\begin{aligned} \dot{x} &= A \cdot x + B \cdot u \\ y &= C \cdot x \end{aligned} \quad (7)$$

where

$$x = \begin{bmatrix} \beta & \gamma & \psi & y_l \end{bmatrix}^T, \quad u = \begin{bmatrix} \delta_f & N_z \end{bmatrix}^T, \quad y = \begin{bmatrix} \gamma & \psi & y_l \end{bmatrix}^T,$$

$$A = \begin{bmatrix} -\frac{2(C_f + C_r)}{m V_x} & -1 - \frac{2(C_f l_f - C_r l_r)}{m V_x^2} & 0 & 0 \\ -\frac{2(C_f l_f - C_r l_r)}{I} & -\frac{2(C_f l_f^2 + C_r l_r^2)}{I V_x} & 0 & 0 \\ 0 & 1 & 0 & 0 \\ V_x & l_{pre} & V_x & 0 \end{bmatrix},$$

$$B = \begin{bmatrix} \frac{2C_f}{m V_x} & \frac{2C_f l_f}{I} & 0 & 0 \\ 0 & \frac{1}{I} & 0 & 0 \end{bmatrix}^T, \quad C = \begin{bmatrix} 0 & 1 & 0 & 0 \\ 0 & 0 & 1 & 0 \\ 0 & 0 & 0 & 1 \end{bmatrix}.$$

1.4 Experimental Vehicle and Onboard Vision System

The experimental vehicle used in this research is a single-seat EV with IWMs. The vehicle structure and sensor configurations are shown in Fig. 2. An accelerometer/gyro-integrated sensor was installed in the vehicle's CoG to provide longitudinal acceleration and yaw rate information. A steering angle sensor was attached to the steering shaft to detect the steering angle and direction. Wheel speed encoders were installed in the front wheels (nondriven wheels) to acquire the vehicle velocity [Nam *et al*. 2012]. To evaluate the estimation results, a noncontact optical sensor was installed for online body slip angle acquisition.

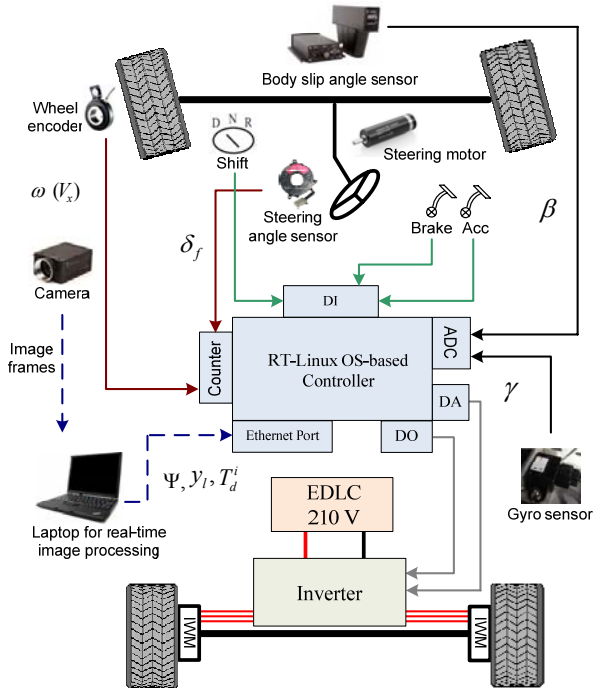

Fig. 2. Vehicle structure and sensor configuration of the experimental vehicle.

The onboard vision system includes a Grasshopper camera produced by Point Grey and a laptop computer for image processing. The frame rate of the camera was set to 30 fps. The images captured by the camera were grabbed by a CARDBUS frame grabber in the laptop and then processed by the image processing program in real time. Depending on incoming images and processor loads, the delay caused by the image processing program varied from 10 ms to 30 ms. That is, image processing delays are within the sampling period of the camera. The final outputs from the vision system are ψ, y_l and T_d^i which were sent to the vehicle controller based on socket programming using UDP protocol, where T_d^i is the the amount of delay, i is the time stamp of visual information ($i = 1, 2, \ldots n$).

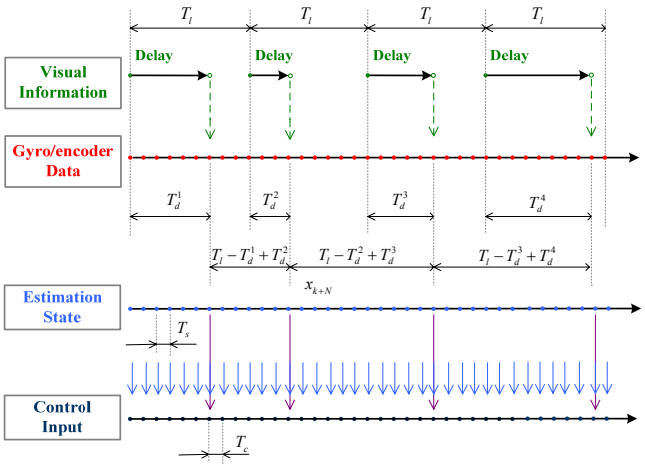

Fig. 3. Time sequences of measurements, estimate and control input.

3. PROBLEM STATEMENT

To apply the Kalman filter in real time, equation (7) needs to be implemented in the discretized form, as shown in (8), where k is the time step. As the system model contains uncertainties and the sensor measurements are contaminated by noises, process noise w_k and measurement noise v_k are also included.

$$\begin{aligned} x_{k+1} &= G_k \cdot x_k + H_k \cdot u_k + w_k \\ y_k &= C_k \cdot x_k + v_k \end{aligned} \tag{8}$$

where

$$G_k = e^{A \cdot T}, \quad H_k = \int_0^T e^{A \cdot \tau} \cdot B d\tau,$$

$$C_k = C, \quad T : sampling\ time$$

Unlike other kinds of onboard sensors, data from vision system is unevenly delayed and the sampling time of a camera is long. The sampling sequence is shown in Fig. 3.

3.1 Multiple Sampling Rates

In the combined system model, two different measurement times are available: the sampling period of yaw rate is short (defined as T_s), and the updating time of visual information is much longer (defined as T_l). Therefore, the selection of T_s and T_l for system discretization needs to be considered. If the system sampling time is set to T_l, data from the high-speed sensors have to be dropped during inter-sampling of the slow-speed device. This is a straightforward solution for the multi-rate issue but obviously deteriorates the estimation performance. An alternative method is to set the system sampling time to T_s; then, all the information from the fast-rate sensors can be utilized. However, as expressed in (9), visual data is not always available at every time step.

$$y_k = \begin{cases} [\gamma_k \quad \psi_k \quad y_{l_k}]^T & if \quad k = \left[(i-1) \cdot T_l + T_d^i \right] / T_s , \\ [\gamma_k \quad 0 \quad 0]^T & if \quad k \neq \left[(i-1) \cdot T_l + T_d^i \right] / T_s . \end{cases} \tag{9}$$

3.2 Uneven Sampled Visual Data

In addition to the multi-rate sampling issue, measurements from the vision system are random delayed because of image processing. Therefore, the visual output equation becomes

$$y_k^{vis} = C \cdot x_{k-n_d^i}^{vis} + v_{k-n_d^i}^{vis} \tag{10}$$

$$where \quad n_d^i = T_d^i / T_s$$

From (10), it can be known that the information from the visual system at step k represents the measurement at step k-

n_d^i. Moreover, n_d^i is not constant due to the change of image processing time. In this research, as T_d^i is assumed to be less than one sampling period of the camera, and n_d^i can only be one value from the set {1, 2, …, 33} at an arbitrary time step *i*. In case of constant and small time delay, augmentation of state vector can be effectively employed. However, it is time consuming and complex for the random delay with large multi-ratio as discussed in this study.

4. KALMAN FILTER CONSIDERING MULTI-RATE AND UNEVEN DELAYED MEASUREMENTS

As aforementioned, with the combined system model, two issues need to be considered for the Kalman filter (KF) design, namely, uneven delayed and multi-rate measurements. Basic Kalman filter principle can be found in [Welch *et al*. 2006] and only the two problems will be addressed in this section.

4.1 Reconstruction of Uneven Delays

The system measurement equation can be expressed separately as

$$y_k^{veh} = C \cdot x_k^{veh} + v_k^{veh} \tag{11}$$

$$y_k^{vis} = C \cdot x_{k-n_d^i}^{vis} + v_{k-n_d^i}^{vis} \tag{12}$$

As the measurements are utilized for residuals calculation, the residuals will be considered instead of the measurements for Kalman filter design in the remainder of this subsection. At step *k*, if the measurements are directly filtered by a Kalman filer, the vehicle model-related residual and vision model-related residual are calculated as (13) and (14), respectively.

$$\varepsilon_k^{veh} = y_k^{veh} - C \cdot \hat{x}_k^{veh-} \tag{13}$$

$$\varepsilon_k^{vis} = y_k^{vis} - C \cdot \hat{x}_k^{vis-} \tag{14}$$

From (11) to (14), it can be observed that, unlike vehicle model-related data, visual information is randomly delayed and therefore can not be used directly for residual calculation. An algorithm that can compensate such random measurement delay is desirable.

First of all, by holding the time update, at step *k*, the residual of step $k - n_d^i$ can be obtained as (15).

$$\varepsilon_{k-n_d^i}^{vis} = y_k^{vis} - C \cdot \hat{x}_{k-n_d^i}^{vis-} \tag{15}$$

Although (15) does not represent the current visual residual, unlike the residual calculation method in (14) which is out of sequence, it is mathematical meaningful in the sense of residual calculation. Then, how to utilize previous residual for current state update should be addressed. A previous method that modifies the Kalman gain can be referred to [Larsen *et al*. 1997]. In this paper, a measurement reconstruction methodology based on residual estimation is developed.

The proposed measurement reconstruction method can be summarized as: consider that the visual data are sampled at $(i\text{-}1)\cdot T_l$, but are not available until time $(i\text{-}1)\cdot T_l+T_{d\_i}$, it is reasonable to assume that the samplings are taken at $(i\text{-}1)\cdot T_l+T_{d\_i}$ instead of $(i\text{-}1)\cdot T_l$. Thus, the delay is removed from the reconstructed sampling sequence. As the measurements at $(i\text{-}1)\cdot T_l+T_{d\_i}$ represent the data at $(i\text{-}1)\cdot T_l$, corresponding modification of residual is necessary. After the above re-arrangement, the delays are removed from the visual measurements. However, the updates are still uneven and the sampling time is much longer than that of the secondary one. The problem is then transformed into designing a multi-rate Kalman filter for a discrete system with random multi-ratio. Two points need to be considered in this case: 1) residual modification at every $(i\text{-}1)\cdot T_l+T_{d\_i}$ time; 2) residuals estimation between every neighbouring primary samples.

4.2 Inter-sampling Residual Design

After reconstruction of visual delays, the sampling time of visual information changes from step to step and can be expressed as

$$T_{smpl}^{vis} = T_l - T_d^{i-1} + T_d^i \tag{16}$$

Aimed at solving the uneven and multi-rate sampling issues, multi-rate Kalman filter is designed. Moreover, the multi-rate Kalman filter takes more information from high-speed sensors and increases the updating rate of the estimator for high-performance control. First, the system is discretized with the sampling time of the fastest device (*T* is set to 1 ms in this research). Next, the time and measurement updates need to be designed. For the time update, the multi-rate Kalman filter can be implemented in the same way as the single-rate one. The camera's sampling period is $T_l - T_d^{i-1} + T_d^i$ and during the sampling intervals, no information from the vision system is available. Therefore, pseudo-corrections have to be implemented for the operation of the measurement update.

The basic idea of the inter-sample residual estimation is to utilize the residual of the initial step that is available and propagate it to the following inter-measurement steps. After $\left(T_l - T_d^{i-1} + T_d^i\right)/T_s$ steps (delayed steps), the residual is recalculated when new measurements come in. The definition of residual ε_k^{vis} and estimation error e_k^{vis} are shown in (17) and (18), respectively.

$$\varepsilon_k^{vis} = y_k^{vis} - C \cdot \hat{x}_k^{vis-} \tag{17}$$

$$e_k^{vis} = x_k^{vis} - \hat{x}_k^{vis} \tag{18}$$

To derive the pseudo-residual algorithm, process noise and measurement noise are assumed to be small and are hence

ignored. This assumption is based on two considerations. First, the inter-sample residual compensation in this application is designed for visual information. As aforementioned, the vision model and the visual measurements are assumed to be accurate. Second, obtaining them in real time for algorithm implementation is difficult.

The algorithm for the inter-sample residual calculation can be generalized in four steps as follows:

1) When sensor measurements are available, the initial residual at step k is obtained as (19). The initial residual is available at each $\left(T_l - T_d^{i-1} + T_d^i\right)/T_s$ step.

$$\varepsilon_k^{vis} = y_k^{vis} - C \cdot \hat{x}_k^{vis-} \tag{19}$$

2) Using (19) and considering that the matrix C might not be invertible, the initial estimation error can be estimated by ε_k^{vis} as

$$e_k^{vis} = \left[\left(C^T \cdot C\right)^{-1} \cdot C^T - K_k^{vis}\right] \cdot \varepsilon_k^{vis} \tag{20}$$

3) From the definition of the estimation error in (18), the estimation dynamics at step $k+j$ can be propagated using (21), where $j \in \left[1, \left(T_l - T_d^{i-1} + T_d^i\right)/T_s\right)$.

$$\begin{aligned} e_{k+j}^{vis} &= x_{k+j}^{vis} - \hat{x}_{k+j}^{vis} \\ &= x_{k+j}^{vis} - \hat{x}_{k+j}^{vis-} - K_{k+j}^{vis} \cdot (y_{k+j}^{vis} - C \cdot \hat{x}_{k+j}^{vis-}) \\ &= (x_{k+j}^{vis} - \hat{x}_{k+j}^{vis-}) - K_{k+j}^{vis} \cdot (C \cdot x_{k+j}^{vis} - C \cdot \hat{x}_{k+j}^{vis-}) \\ &= (I - K_{k+j}^{vis} \cdot C) \cdot G_{k+j-1}^{vis} \cdot e_{k+j-1}^{vis} \end{aligned} \tag{21}$$

4) Finally, the pseudo-residual during the inter-sampling period is given by (22), and it is updated using (21).

$$\begin{aligned} \tilde{\varepsilon}_{k+j}^{vis} &= y_{k+j}^{vis} - C \cdot \hat{x}_{k+j}^{vis-} \\ &= C \cdot x_{k+j}^{vis} - C \cdot {}^{vis-}_{k+j} \\ &= C \cdot G_{k+j-1}^{vis} \cdot e_{k+j-1}^{vis} \end{aligned} \tag{22}$$

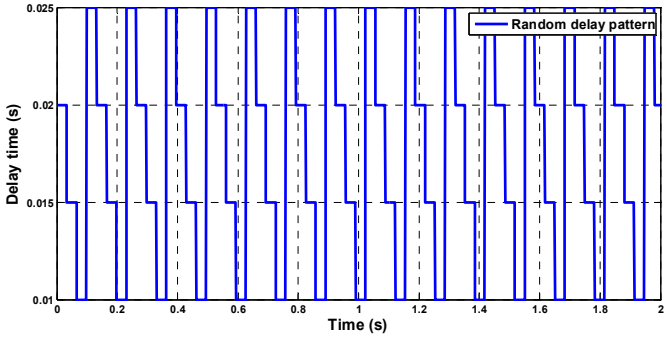

Fig. 4. Random delay pattern in simulation.

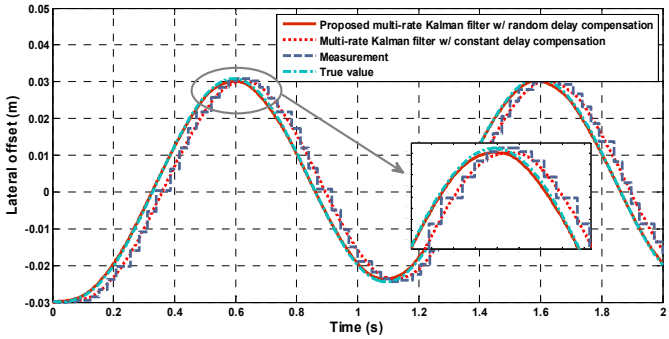

Fig. 5. Estimation methods comparison in simulation.

The first two steps are the initialization, and the estimation error is then self-propagated using (21). Finally, the inter-sample residuals are obtained using the estimated error dynamics. The estimation errors must be noted to be unknown in reality because some states are not available from the sensors. In this algorithm, the estimation errors function as intermediate quantities for the calculation of pseudo-residuals.

5. SIMULATION AND EXPERIMENT

The performance of the proposed multi-rate Kalman filter was compared with the other methods in simulation. The vehicle was assumed to run at a speed of 25 km/h, and a sinusoidal steering input was given. To simulate real conditions, the vehicle model and the Kalman filter model were made different from each other: the real C_f and C_r were set as 1.2 times larger than the estimator ones. The random delay pattern was shown in Fig. 4, where the delay time is repeated as {20ms, 15ms, 10ms, 25ms}. The performance of the proposed method is shown in Fig. 5. For comparison, a method that assumes a constant delay is also provided. As can be observed, the measurement is random delayed and held; if a constant delay is assumed, the estimation performance is not satisfying. Meanwhile, the proposed multi-rate Kalman filter with measurement reconstruction and inter-sample compensation provided the best estimation result compared with the other methods.

Field tests were conducted with our experimental vehicle for realistic verification of the proposed estimator. A sinusoidal steering input was provided by the driver, and the vehicle speed varied from 0 km/h to 30 km/h during the operation. Similar to the simulation settings, the C_f and C_r of the Kalman filter model were made different from those of the real vehicle. In fact, the true vehicle model can not be exactly known in all driving conditions. The varying image processing time during one experiment is shown in Fig. 6. As can be observed, the processing time during the test varied from 9 ms to 18 ms, and can be obtained from the onboard vision system. The proposed multi-rate Kalman filter with measurement reconstruction and residual compensation was compared with the constant delay method in Fig. 7. The multi-rate Kalman filter with constant delay compensation could not provide delay-free estimate as the proposed approach.

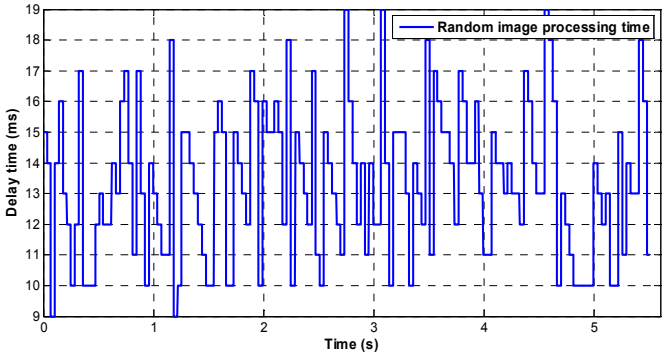

Fig. 6. Uneven image processing time during a test.

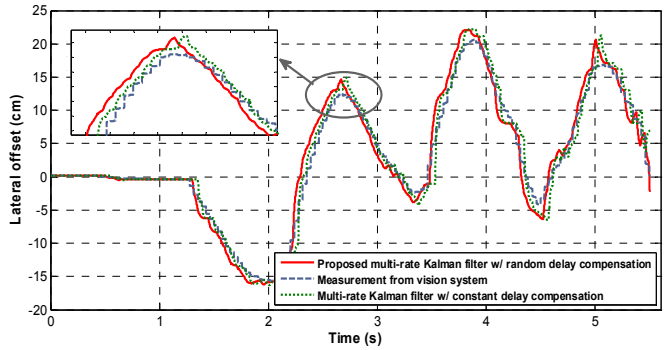

Fig. 7. Estimation comparisons based on experimental data.

6. CONCLUSIONS

In this paper, to improve the motion control performance for EVs, a multi-rate Kalman filter with measurable random time delay compensation was proposed. With the proposed method, measurable random time delay and sampling discrepancy issues were solved. In this paper, first of all, a combined vehicle and vision model was derived and the experimental setups were introduced. Then, the multi-rate and uneven time-delay issues were explained and formulated. For measurable uneven visual information delay, a measurement and Kalman gain reconstruction method was employed, and then, aimed at solving the uneven and multi-rate sampling issues, multi-rate Kalman filter is designed. Finally, in the simulation and experiment section, the proposed multi-rate Kalman filter was compared with the fixed-delay method. The proposed methodology is updated much faster than traditional approach for onboard vision system [2007], and therefore can be applied to high performance motion control systems for EVs.

REFERENCES

Aoki Y., Uchida T. and Hori Y. (2005). Experimental Demonstration of Body Slip Angle Control based on a Novel Linear Observer for Electric Vehicle. IECON *2005, 31st Annual Conference of IEEE*, pp. 6-10.

Bertozzi M. and Broggi A. (1998). GOLD: A Parallel Real-time Stereo Vision System for Generic Obstacle and Lane Detection. IEEE Trans. Image Process, Vol. 7, pp. 62-81.

Cerone V., Milanese M. and Regruto D. (2007). Experimental Results on Combined Automatic Lane Keeping and Driver's Steering. *American Control Conference, 2007*, pp. 3126-3131.

Cerone V., Milanese M. and Regruto D. (2009). Combined Automatic Lane-Keeping and Driver's Steering Through a 2-DOF Control Strategy. *IEEE Trans. Control Syst. Technol.*, vol. 17, no. 1, pp. 135-142

Choi M., Choi J., Park J. and Chung W. K. (2009). State Estimation with Delayed Measurements considering Uncertainty of Time Delay. *Proc. ICRA 2009*, pp. 3987–3992.

Fujimoto H., Takahashi N., Tsumasaka A. and Noguchi T. (2006). Motion Control of Electric Vehicle based on Cornering Stiffness Estimation with Yaw-Moment Observer. In proceeding of Advanced Motion Control, 9th IEEE International Workshop on, pp. 206-211.

Kim B. and Peng H. (2012). Vehicle Stability Control of Heading Angle and Lateral Deviation to Mitigate Secondary Collisions. The 11th International Symposium on Advanced Vehicle Control, Seoul, Sept. 2012.

Larsen T. D., Andersen N. A., Ravn O. and Poulsen N. K. (1998). Incorporation of Time Delayed Measurements in a Discrete-time Kalman Filter. *In Proceedings of the 37th IEEE Conference on Decision & Control*, pp. 3972-3977.

McCall J. C. and Trivedi M. M. (2006). Video-based Lane Estimation and Tracking for Driver Assistance: Survey, System, and Evaluation. IEEE Trans. Intell. Transp. Syst., Vol. 7, pp. 20-37, 2006.

Nam K., Fujimoto H. and Hori Y. (2012). Lateral Stability Control of In-Wheel-Motor-Driven Electric Vehicles Based on Sideslip Angle Estimation Using Lateral Tire Force Sensors. *IEEE Trans. Veh. Technol.*, vol. 61, no. 5, pp. 1972-1985.

Wang Y., Nguyen B. M., Kotchapansompote P., Fujimoto H. and Hori Y. (2012). Vision-based Vehicle Body Slip Angle Estimation with Multi-rate Kalman Filter considering Time Delay. *Industrial Electronics (ISIE), 2012 IEEE International Symposium on*, pp. 1506-1511.

Welch G. and Bishop G. (2006). An Introduction to the Kalman Filter, University of North Carolina at Chapel Hill.